RSC Advances

PAPER

View Article Online
View Journal | View Issue

Cite this: *RSC Adv.*, 2021, **11**, 210

Preparing, optimising, and evaluating chitosan nanocapsules to improve the stability of anthocyanins from *Aronia melanocarpa*†

Mingyue Wang,[a] Li Li,[a] Meizhi Wan,[a] Yang Lin,[b] Yuqi Tong,[a] Yanmin Cui,[a] Haotian Deng,[a] Chang Tan,[a] Yanwen Kong[a] and Xianjun Meng *[a]

The anthocyanins extracted from *Aronia melanocarpa* are of great interest because of their potential health-related functionalities. However, their poor stabilities have limited their use in applications. Hence, to improve their physical and oxidative stability, we optimised the chitosan nanocapsules encapsulating anthocyanins from *Aronia melanocarpa*, and evaluated the systems in terms of their physicochemical characteristics, physical and oxidant stability in simulated gastrointestinal digestion and different storage environments. Results show that the obtained nanocapsules present favorable particle size (197 nm) with good surface morphology, highly encapsulation efficiency (65.7%), suitable zeta potential (+42.7 mV), and low polydispersity index (0.032). Furthermore, compared with free anthocyanins, the nanoencapsulated anthocyanins exhibited significantly slower degradation and stronger antioxidant activity during the simulated gastrointestinal digestion and environmental storage. Thus, the physical and oxidative stability of anthocyanins in *Aronia melanocarpa* was enhanced significantly by chitosan nanoencapsulation.

Received 24th September 2020
Accepted 9th December 2020

DOI: 10.1039/d0ra08162k

rsc.li/rsc-advances

1 Introduction

Aronia melanocarpa, a shrub also known as the black chokeberry, has been reported to be a rich source of plant anthocyanins (ANT). ANT are known for their biological activity toward reducing chronic diseases such as diabetes, obesity, heart and circulatory diseases, nervous system disorders, and cancer.[1–4] However, ANT are highly sensitive to environmental and chemical factors such as temperature, exposure to oxygen, light and enzymatic degradation, all of which limit the use of ANT in food applications.[5,6]

To enhance their physical and oxidative stability, it is therefore demonstrated that nanoencapsulation techniques could protect the ANT from environmental and gastrointestinal degradation.[7,8] However, different plant has their different ANT composition, it is necessary to verify whether the chosen delivery system will benefit to obtain nanocapsules capable of improving their stability.

Chitosan (CS) has received significant attention for use as a biopolymer in nanoencapsulation drug delivery. This natural polysaccharide is obtained from crustacean shells *via* the deacetylation of chitin and is considered particularly attractive as a wall material for nanoencapsulation owing to its biodegradability, biocompatibility, and lack of toxicity.[9] Because CS is a cationic polymer, it can be cross-linked with the negatively charged groups of polyanions such as tripolyphosphate (TPP). TPP is commonly used as a cross-linking agent in ionic gelation because it is non-toxic, does not require organic solvents, and is readily controllable during the linking process.[10,11]

To date, the ionic cross-linking of CS with TPP, both food-safe compounds, has been applied to the delivery and encapsulation of proteins, genes, drugs, vitamins, and various phenolic compounds.[12] However, to the best of our knowledge, there is no reported study on the nanoencapsulation of ANT extracted from *Aronia melanocarpa*.

Therefore, our study focused on the preparation and optimisation of nanocapsules to create a delivery system for ANT extracts from *Aronia melanocarpa*. The optimum nanoencapsulation conditions were modeled using a Box–Behnken design (BBD) based on response surface methodology (RSM) toward minimizing nanoparticle size and maximizing encapsulation efficiency (EE). The obtained nanoparticles were characterized by particle size and zeta potential analysis, transmission electron microscopy (TEM), and Fourier-transform infrared (FT-IR) spectroscopy. Moreover, we examined the effects of *in vitro* digestion, storage and light on the physical and oxidative stability of nanocapsules compared to free anthocyanins.

[a]*College of Food, Shenyang Agricultural University, No. 120 Dongling Road, Shenhe District, Shenyang City 110866, People's Republic of China*

[b]*Department of Food Science and Technology, Zhejiang University of Technology, Hangzhou 310014, Zhejiang, People's Republic of China*

† Electronic supplementary information (ESI) available. See DOI: 10.1039/d0ra08162k

2 Materials and methods

2.1 Materials

Fresh *Aronia melanocarpa* was harvested in September 2019 and obtained from the Liaoning Fu KangYuan Black Chokeberry Technology (40°47′41″N, 122°40′42″E, Haicheng, Liaoning, China). Medium molecular weight CS (deacetylation degree: 75–85%) and TPP were purchased from Sigma–Aldrich (Steinheim, Germany). 2,2-Diphenyl-1-picrylhydrazyl (DPPH), acetonitrile, formic acid and potassium ferricyanide were purchased from Dingguo Biological Technology Co., Ltd. (Shenyang, Liaoning, China).

2.2 Extracting the anthocyanins

The anthocyanins extraction and purification steps were performed according to the method developed by Meng *et al.* with some modifications.[13] Prior to use, the samples were stored at −80 °C in an ultralow-temperature freezer. Next, 500 g of *Aronia melanocarpa* was washed and homogenised using a juicer. The samples were then extracted with 55% (v/v) ethanol with 0.1 vol% HCl at 45 °C for 90 min, with a 1 : 44 material-to-solvent ratio, in an ultrasonication bath (KQ-700DV, Kunshan Ultrasonic Instruments, Jiangsu, China) at 400 W. The extraction solvent was removed by rotary evaporation (RE-5203A, Shanghai Bilon Instruments, Shanghai, China) at 45 °C until no alcohol remained in the sample, and the remaining anthocyanins extract was purified by NKA-9 absorbent resin (Beijing Solarbio Science and Technology Co., Ltd., Beijing, China). The obtained purified anthocyanins extract was lyophilised in a vacuum freeze-dryer. Then anthocyanins extract was further purified by semipreparative reverse-phase high-performance liquid chromatography (RPLC). All of anthocyanins absorption peaks were collected in a fraction collector. The extraction solvent was removed using rotary evaporation, and then the compounds were freeze-dried.

2.3 Determining anthocyanins content

The anthocyanins content was determined using the pH-differential method as the cyaniding-3-glucoside equivalents using the following equation:

$$\text{Anthocyanins content, mg L}^{-1}) = (\Delta A \times M \times F \times 10^3)/\varepsilon \times 1 \quad (1)$$

where $\Delta A = (A_{520\text{nm}} - A_{700\text{nm}})_{\text{pH 1.0}} - (A_{520\text{nm}} - A_{700\text{nm}})_{\text{pH 4.5}}$; M (molecular weight) = 449 g mol^{-1} for cyanidin-3-glucoside; F = dilution factor; 10^3 = conversion from gram to milligram; ε (molar extinction coefficient) = 26 900; 1 = path length in cm.

The anthocyanins were qualified and quantified by HPLC-DAD-ESI-MS^2 and found to contain cyanidin-3-*O*-galactoside, cyanidin-3-*O*-arabinoside, cyanidin-3-*O*-glucoside, and cyanidin-3-*O*-xyloside (ESI). The total concentration of anthocyanins in *Aronia melanocarpa* was 938.72 mg g^{-1}.

2.4 Preparing the nanocapsules

Nanocapsules were formed using the ionic gelation method.[14] Briefly, CS was dissolved in a 1 vol% aqueous acetic acid solution to concentrations of 1.5–3.5 mg mL^{-1}. TPP was then dissolved in distilled water to concentrations of 0.5–1.5 mg mL^{-1}. CS void nanoparticles were formed by adding the TPP solution dropwise to the CS solution under magnetic stirring (7200 rpm, 1 h). The final pH of the mixed solution was adjusted to 4.6–4.8 using 0.5 mol L^{-1} NaOH. For the nanoencapsulation of *A. melanocarpa* ANT, the amount of ANT (3–9 mg) in methanol was prepared and slowly dripped into the CS solution with continuous stirring (7200 rpm) at room temperature (25 °C). After 10 min of ANT addition, the TPP solution was added dropwise into the mixture. To remove unencapsulated ANT, the system was dialyzed against distilled water for 3 h using a dialysis bag (molecular weight cutoff = 8000 Da). Subsequently, the system was vacuum freeze-dried for 24 h to obtain the ANT-NPs (ANT nanocapsules).

2.5 RSM optimisation design

To elucidate the influence of various variables and optimum preparation conditions, a three-factor, three-level BBD based on RSM was used with Design-Expert software (version 8.0.6, Stat-Ease, Minneapolis, MN, USA). The response surface regression model was fitted to correlate the relationships between responses and independent variables using the following second-order polynomial equation:

$$Y = \beta_0 + \sum_{j=1}^{k} \beta_j X_j + \sum_{j=1}^{k} \beta_{jj} X_j^2 + \sum_{i} \sum_{<j=2}^{k} \beta_{ij} X_i X_j \quad (2)$$

where Y is the predicted response (particle size or encapsulation efficiency); β_0, β_j, β_{jj}, and β_{ij} are the regression coefficients of the constant, linear, quadratic, and interactions terms, respectively; X_i and X_j are the independent variables; and k is the number of independent parameters.

2.6 Determining encapsulation efficiency

EE was determined by separating the non-entrapped ANT by centrifugation at 10 000*g* and 4 °C for 10 min. All measurements were performed in triplicate. EE was calculated as follows:

$$\text{EE (\%)} = (\text{total anthocyanins content} - \text{free anthocyanins content})/ (\text{total anthocyanins content}) \times 100. \quad (3)$$

Here, "total anthocyanins content" is the initial ANT content added to the nanocapsules and "free anthocyanins content" is the ANT content determined in the supernatant.

2.7 Characterizing the nanocapsules

2.7.1 Analysis of morphology, particle size, zeta potential and polydispersity index. The morphologies of the ANT-NPs were examined by TEM (JEM-F200, Jeol, Tokyo, Japan). The samples were prepared by placing tiny drops of a diluted suspension of the nanocapsules onto copper grids coated with

a support film, which were subsequently dried at room temperature prior to examination.

Particle size, zeta potential, and polydispersity index (PDI) were measured with a Zetasizer Nano ZS 90 instrument (Malvern Instruments, Malvern, UK) using the dynamic light scattering (DLS) technique at a fixed scattering angle of 90° at 25 ± 1 °C.

2.7.2 FT-IR spectroscopy. The freeze-dried samples were mixed with anhydrous potassium bromide and compressed into thin disk-shaped pellets. Spectra were acquired on an FT-IR spectrophotometer (Thermo Fisher Nicolet iS20, Waltham, MA, USA) in the 400–4000 cm^{-1} range at a resolution of 4 cm^{-1}.

2.8 Physical and oxidative stability of nanocapsules

The physical stabilities of the free ANT and ANT-NPs were determined by measuring changes in retention rates. The oxidative stabilities of the non-loaded NPs, ANT-NPs, and free ANT were examined using DPPH and FRAP assays.

2.8.1 DPPH radical scavenging activity. The DPPH scavenging method as previously described with some modification.[15] Briefly, 3 mg samples were mixed with 2 mL DPPH solution (0.1 mM), vigorously shaken and incubated in the dark for 30 min (25 °C). Afterwards, the solution absorbance was measured at 517 nm using ethanol as a blank by UV-vis spectrophotometer. The antioxidant activity of the samples was calculated by the following equation:

$$\text{DPPH scavenging activity (\%)} = (A_c - A_s)/A_c \times 100. \quad (4)$$

In which A_c is the absorbance of the control and A_s represents the absorbance of the test sample.

2.8.2 Ferric reducing antioxidant power. The FRAP assay was performed as follows: 1 mL of sample mixed with 2.5 mL of phosphate buffer (0.2 M, pH 6.6) was incubated with potassium ferricyanide (1%, w/v) at 50 °C for 20 min. After cooling, 2.0 mL of trichloroacetic acid (10%, w/v) was added to the mixture followed by centrifugation at 3000 rpm for 10 min. The obtained supernatant was treated with ferric chloride (0.1%, w/v) solution and its absorbance was measured at 700 nm.

2.8.3 *In vitro* digestion studies. *In vitro* digestion studies under simulated mouth, stomach and intestine conditions was analyzed by a static model.[16,17] The simulated saliva fluid (SSF) contained 0.2% of α-amylase in phosphate buffered saline and adjusted to pH 6.8. The simulated gastric fluid (SGF) contained 3.2 mg mL^{-1} pepsin solution, mucin 1.0 mg mL^{-1}, 9.0 mg mL^{-1} NaCl and adjusted to pH 1.8 using 1.0 mol L^{-1} HCl. The simulated small intestinal fluid (SIF) containing 10 mg mL^{-1} pancreatin and 3 mg mL^{-1} bile salts and adjusted to pH 6.8 using 0.5 mol L^{-1} of $NaHCO_3$. Powder samples (100 mg) were placed in a water bath shaker (120 rpm) at 37 °C. The samples were digested sequentially as follows: mouth – addition of 10 mL of SSF and mixing for 5 min; stomach – addition of 10 mL of SGF and mixing for 2 h; and intestines – addition of 10 mL SIF and mixing for 2 h. At designed time intervals (5, 30, 60, 120, 180, 240 min), the ANT content, DPPH scavenging activity and FRAP assays were measured by the method described above. The ANT retention rate was determined using eqn (5):

$$\text{retention rate (\%)} = C_t/C_0 \times 100 \quad (5)$$

where C_0 is the initial content of ANT, and C_t is the content of ANT at time t.

2.8.4 Storage studies. Storage studies were performed at three different conventional temperatures corresponding to freezer (−20 °C), refrigerator (4 °C), and room temperature (25 °C) and stored in the dark for 25 d. Furthermore, we investigated the effect of a higher temperature (40 °C) on ANT stability in the dark for 5 days.

2.8.5 Photo studies. Samples were irradiated in a SHP150 illumination incubator (Samsung Laboratory Instrument Co., Shanghai, China) with fluorescent lamps at an illumination intensity of 5000 ± 500 l× for 5 days at 25 °C.

2.9 Statistical analysis

All experiments were performed at a minimum of three times. Statistical analysis during the optimisation of the ANT-NPs was performed by analysis of variance (ANOVA) using Design-Expert software. LSD and Duncan's comparison was carried out to determine significant differences ($p < 0.05$) using SPSS software (version 19.0, SPSS, Chicago, IL, USA).

3 Results and discussion

3.1 RSM design

3.1.1 Modelling the polyphenol nanoencapsulation process. To determine the minimum particle size and maximum EE, a three-level BBD with three factors was selected to optimise the ANT nanoencapsulation process. The particle sizes (Y_1) and EEs (Y_2) obtained from 17 runs are presented in

Table 1 Compositions and responses in the Box–Behnken design (BBD)[a]

	Independent variables			Responses	
Run	X_1	X_2	X_3	Y_1	Y_2
1	3.5	1.5	6	299	53.4
2	2.5	1.5	3	384	55.3
3	2.5	0.5	3	280	44.3
4	1.5	1	9	664	40.5
5	3.5	0.5	6	263	51.5
6	1.5	0.5	6	419	37.9
7	2.5	1	6	220	65.8
8	3.5	1	3	342	50.2
9	1.5	1	3	447	49.6
10	2.5	1	6	237	62.7
11	2.5	1	6	197	63.9
12	2.5	0.5	9	255	46.1
13	3.5	1	9	271	57.8
14	2.5	1.5	9	546	41.4
15	2.5	1	6	209	64.4
16	1.5	1.5	6	611	59.1
17	2.5	1	6	203	60.1

[a] X_1: chitosan concentration (mg mL^{-1}); X_2: sodium tripolyphosphate concentration (mg mL^{-1}); X_3: anthocyanins amount (mg); Y_1: particle size (nm); Y_2: encapsulation efficiency (%).

Table 2 ANOVA data for the quadratic response models of all independent variables[a]

	Particle size (nm)					Encapsulation efficiency (%)				
Factor	Sum of squares	df	Mean square	*F*-value	*p*-Value	Sum of squares	df	Mean square	*F*-value	*p*-Value
Model	3.402×10^5	9	37 799.71	57.45	<0.0001**	1205.84	9	133.98	11.69	0.0019**
X_1	1.663×10^5	1	1.663×10^5	252.76	<0.0001**	190.16	1	190.16	16.59	0.0047**
X_2	50 570.08	1	50 570.08	76.86	<0.0001**	197.64	1	197.64	17.25	0.0043**
X_3	27 170.08	1	27 170.08	41.30	0.0004**	76.51	1	76.51	6.68	0.0363*
X_1^2	65 552.84	1	65 552.84	99.63	<0.0001**	108.55	1	108.55	9.47	0.0179*
X_2^2	15 170.53	1	15 170.53	23.06	0.0020**	257.98	1	257.98	22.51	0.0021**
X_3^2	36 436.42	1	36 436.42	55.38	0.0001**	324.40	1	324.40	28.31	0.0011**
X_1X_2	6084.00	1	6084.00	9.25	0.0188*	93.12	1	93.12	8.13	0.0247*
X_1X_3	20 736.00	1	20 736.00	31.52	0.0008**	69.72	1	69.72	6.08	0.0430*
X_2X_3	8742.25	1	8742.25	13.29	0.0082**	61.62	1	61.62	5.38	0.0535^{ns}
Lack of fit	3608.75	3	1202.92	4.83	0.0812^{ns}	61.83	3	20.61	4.48	0.0906^{ns}
Pure error	996.80	4	249.20			18.39	4	4.60		
CV	7.46					6.37				
R^2	0.9866					0.9376				

[a] X_1: chitosan concentration (mg mL^{-1}); X_2: sodium tripolyphosphate concentration (mg mL^{-1}); X_3: amount of anthocyanins (mg); Y_1: particle size (nm); Y_2: encapsulation efficiency (%); CV: coefficient of variation; R^2: coefficient of determination. **significant $p < 0.01$. *significant $p < 0.05$. ns: not significant $p > 0.05$.

Table 1. The response values for Y_1 and Y_2 varied from 197 to 664 nm and 37.9 to 65.8%, respectively. To establish the significant variables that affect particle size and EE, the R^2, F, and p values were also determined (Table 2). The suitability of the quadratic model was demonstrated by R^2 values of 0.9866 and 0.9376 for particle size and EE, respectively, which suggest the experimental and predicted data are in agreement. Furthermore, the insignificant lack of fit value ($p_{if} > 0.05$) highlights the adequacy of all response surfaces.[18–20]

3.1.2 Effect of independent variables on particle size and encapsulation efficiency. The effect of each independent variable on particle size is described by eqn (6) and shown in the corresponding 3D response surface plots (Fig. 1A–C).

$$\text{Particle size} = 304.77 - 122.76X_1 + 97.38X_2 + 71.38X_3 - 19.50X_1X_2 - 36.00X_1X_3 + 46.75X_2X_3 + 31.19X_1^2 + 60.02X_2^2 + 93.02X_3^2 \quad (6)$$

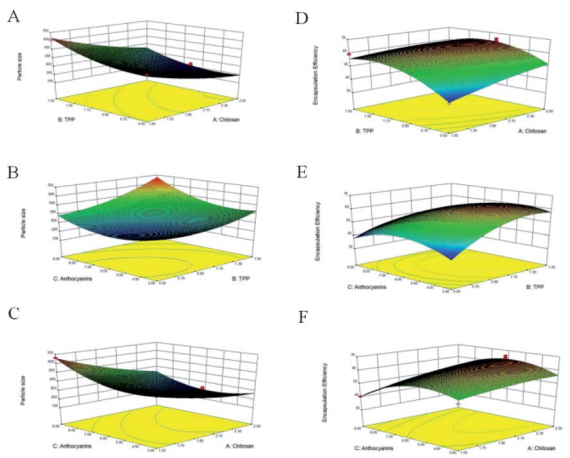

Fig. 1 3D-response surface plots illustrating the effect of independent variables on particle size (nm) and encapsulation efficiency (EE, %): (A and D) chitosan (CS) and tripolyphosphate (TPP); (B and E) TPP and anthocyanins (ANT); and (C and F) CS and ANT.

where X_1 and X_2 are the independent variables for the concentration of CS and TPP, respectively, and X_3 is the amount of anthocyanins.

Through regression analysis, the results (Table 2) revealed that particle size was affected significantly by X_1, X_2, and X_3 at the $p < 0.01$ level. The secondary terms, namely X_1^2, X_2^2, and X_3^2, were statistically significant at the $p < 0.01$ level, and the effects of both X_1X_3 and X_2X_3 were determined to be more significant than that of X_1X_2 at the $p < 0.01$ level. As illustrated, particle size fell in the 197–664 nm range and decreased with increasing CS (X_1) and TPP (X_2) concentrations to the midpoint of the response plot, above which particle size increased. Lower concentrations of either CS or TPP led to the formation of small nanocapsules. Similar results were observed in a study on the microencapsulation of lung proteins by Grenha *et al.*,[21] who reported that particle size increased with increasing amount of added CS solution, which was attributed to the higher CS concentration that causes strong hydrogen bonding interactions and thereby hinders the formation of small nanoparticles with TPP.

The second-order polynomial equation expressed by eqn (7) and the corresponding 3D response surfaces (Fig. 1E–G) illustrate the interaction of each independent variable with EE.

$$\text{EE} = 60.50 + 4.15X_1 + 6.09X_2 - 3.79X_3 - 2.41X_1X_2 + 2.09X_1X_3 - 3.92X_2X_3 - 1.27X_1^2 - 7.83X_2^2 - 8.78X_3 \quad (7)$$

The data in Table 2 reveal that only the X_2X_3 interaction term does not significantly affect EE. The quadratic terms X_2^2 and X_3^2 are more significant at the $p < 0.01$ level, while X_1^2 is significant at the $p < 0.05$ level. EE increased with each variable until the midpoint, above which EE decreased (Fig. 1E–G). For example, an increase in ANT amount from 3 to 6 mg increased EE, but at higher amount, EE decreased. Consistently, Hu *et al.*,[22] studied CS-TPP nanoparticles for the delivery of tea catechins and reported that EE increased as the amount of tea catechins was

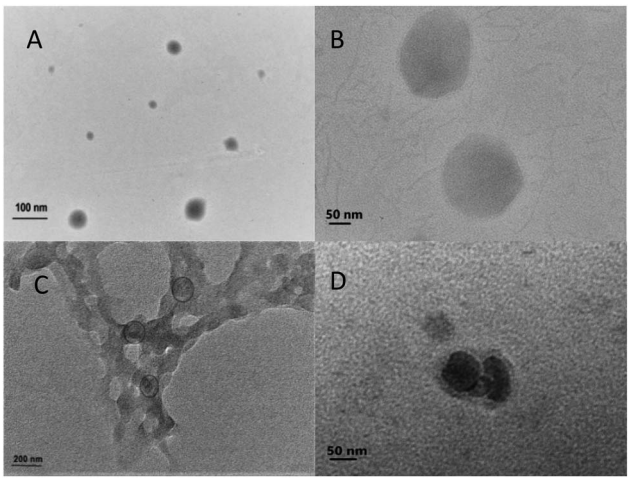

Fig. 2 TEM images of (A and B) non-loaded nanocapsules and (C and D) ANT-NPs.

increased from 1 to 3%, and then decreased at higher amounts, consistent with our observations. This trend may be due to the high cross-linking density between CS and the loaded extract.

3.1.3 Optimisation and validation. Based on the RSM model, and with the aim of attaining minimum particle size and maximum EE, the optimum conditions of each parameter were determined as follows: CS concentration $X_1 = 2.5$ mg mL^{-1}, TPP concentration $X_2 = 0.9$ mg mL^{-1}, and ANT amount $X_3 = 5.7$ mg. The resulting average particle size and EE were determined to be 196.4 nm (Fig. 3) and 65.7%, respectively, which were in reasonable agreement with the corresponding predicted values of 202 nm and 62.8%.

3.2 Nanocapsules characterisation

3.2.1 Morphology, particle size, and zeta potential. The ANT-NPs were synthesised by ionic cross-linkage between the positively charged amino groups in CS and the negatively charged phosphate groups in TPP. Physicochemical characterisation of the ANT-NPs revealed their structures and interactions, which are essential for their use in various applications.[23,24]

TEM images of non-loaded NPs and ANT-NPs obtained under the optimised preparation conditions are displayed in Fig. 2. The non-loaded nanocapsules exhibit spherical morphologies with diameters below 100 nm, while those of ANT-NPs were 100–200 nm. It is considered that by adding ANT into chitosan nanocapsules leads to the formation of cross-link between chitosan and ANT resulted in a larger size distribution.[25] However, non-loaded NPs and ANT-NPs are 102.6 nm and 196.5 nm in size, respectively, as determined by DLS, which are larger than the values determined by TEM. These discrepancies are possibly due to swelling of the CS layers of the nanocapsules in the presence of water, with DLS measuring hydrodynamic diameter, whereas TEM provides the actual diameter of the dried nanocapsule.[26,27] Furthermore, both non-loaded NPs and ANT-NPs exhibited narrow particle-size distributions, as indicated by their PDIs of 0.047 and 0.032, respectively; these low PDIs accurately reflect the homogeneities of the nanocapsules.[28]

The zeta potentials of the nanocapsules were determined as an indicator of their stabilities. Generally, a high zeta potential reflects physical stability induced by electrostatic repulsion, which prevents nanocapsule aggregation.[29] Fig. 2B and D shows that the zeta potential of the non-loaded NPs and ANT-NPs are +43.5 mV and +42.7 mV, which indicates that they are very physically stable.

3.2.2 FT-IR spectroscopy. FT-IR spectroscopy was used to confirm the presence of cross-linking and structural changes in the prepared nanocapsules. The FT-IR spectra of CS, ANT, non-loaded nanocapsules, and ANT-NPs are displayed in Fig. 4. The FT-IR spectrum of CS displays C–OH, C=O, amide II, C–H, and –NH_2 peaks at 1078, 1424, 1631, 2869, and 3425 cm^{-1},

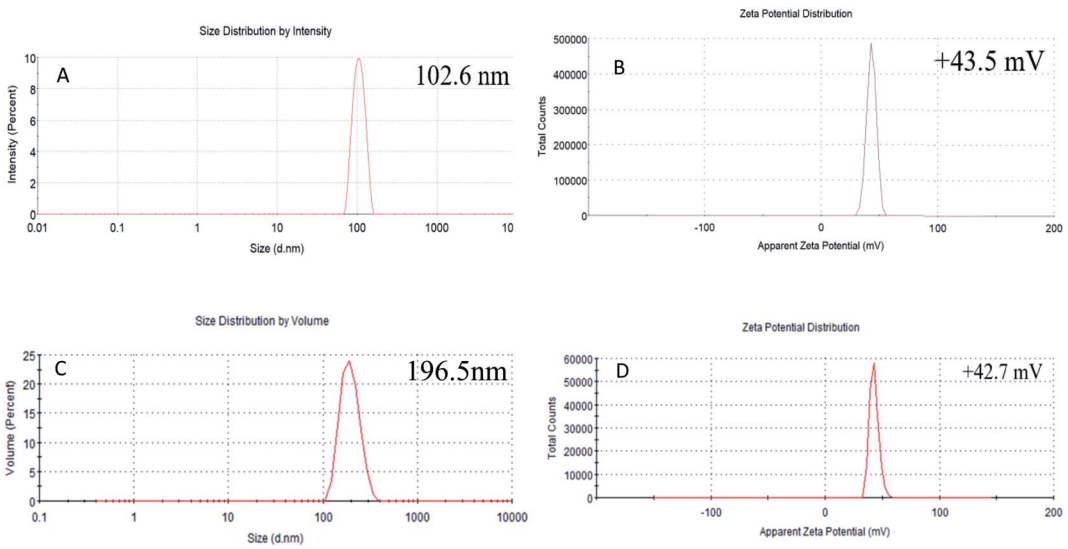

Fig. 3 Particle sizes and zeta potentials of (A and B) non-loaded NPs and (C and D) ANT-NPs.

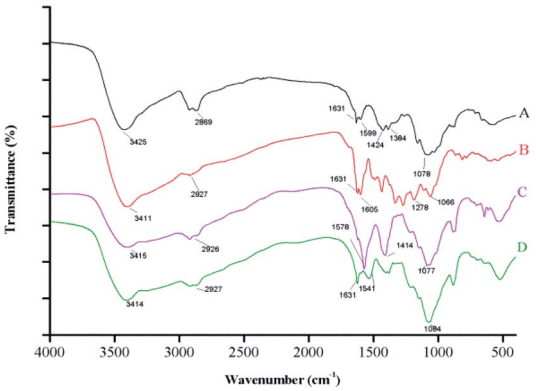

Fig. 4 FT-IR spectra of (A) CS, (B) ANT, (C) non-loaded nanocapsules, and (D) ANT-NPs.

respectively. The spectrum of free ANT shows a peak at 3411 cm^{-1} that corresponds to –OH stretching vibrations, a strong peak at 2927 cm^{-1} assigned to C–H stretching, and a characteristic C–O peak located at 1196 cm^{-1}.

The spectra of the non-loaded nanocapsules and the ANT-NPs overlapped at similar frequencies; the former reveals a shift in the amide II peak, from 1631 to 1578 cm^{-1}, compared to that of free CS, which confirms that the amino groups of CS are linked to the phosphate groups of TPP. Similar result was in accordance with a previous study that nanoencapsulation by ionic gelation method.[30,31] Moreover, it can be observed that the absorption bands of the ANT-NPs are narrow when compared with the non-loaded nanocapsules, which suggested that reciprocity between the amino or carbonyl groups of CS and the phenolic groups of ANT. Notably, a new band was detected in the FTIR spectrum of ANT-NPs at 1541 cm^{-1}, which is associated with aromatic ring vibrations, confirming that the ANT was successfully entrapped in the ANT-NPs. These results further confirm the successful preparation of the ANT-NPs.

3.3 Physical and oxidant stabilities of the nanocapsules

3.3.1 *In vitro* digestion studies. *In vitro* digestion is important when assessing the potential of nanocapsules for delivering anthocyanins *via* food or as a supplement for humans.[32] Fig. 5A shows the retention rates of anthocyanins from ANT-NPs and the behaviour of free ANT during simulated gastrointestinal digestion, while Fig. 5B shows the antioxidant activities of ANT-NPs, ANT, and non-loaded NPs, and Fig. 5C shows the particle size and zeta potential of ANT-NPs.

The digestion process was divided into mouth, gastric, and intestinal phases in this study. Fig. 5A shows that there was no obvious release from both free ANT and ANT-NPs during mouth digestion, which may be due to the short exposure process and the absence of some specific enzymes.[33] The retention rate of the ANT (96.24%) in ANT-NPs was clearly higher than that of free ANT (88.21%) when the samples were subjected to gastric digestion for 1 h. The retention rate of the ANT-NPs was more than 92%, while that of the free ANT was only 76% at the end of the gastric digestion period, which is significantly lower than those obtained from the ANT-NPs. Moreover, the retention rate

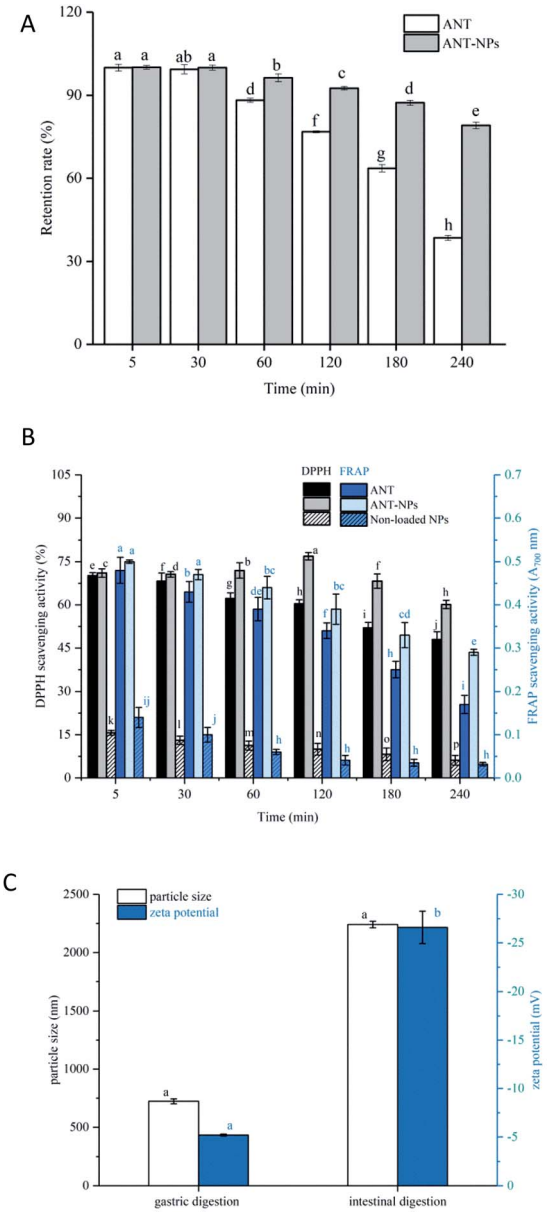

Fig. 5 (A) Retention rates and (B) antioxidant activities of various formulations during *in vitro* digestion. (C) Particle size and zeta potential of ANT-NPs during *in vitro* digestion. Data are expressed as means ± standard deviations (n = 3). Samples designated with different letters indicate significant differences (Duncan, $p < 0.05$).

of free ANT decreased rapidly to 38.52%, while that of ANT-NPs was 79.13% after simulated intestinal digestion. According to the abovementioned results, ANT-NPs exhibit a significantly lower release rate than free ANT under simulated gastrointestinal digestion. When combined with the results shown in Fig. 5C, the particle size and zeta potential of the ANT-NPs clearly change greatly during intestinal digestion, from original small stable particles to large unstable ones. This effect may be due to the fact that chitosan is readily dissolved under strong acid condition, which results in the relaxation of the ANT-NP structure.

To evaluate oxidative stability during digestion, the ANT-NPs were assayed by DPPH and FRAP, the results of which are compared with those of free ANT and the non-loaded NPs. The DPPH assay is usually used to evaluate the antioxidant activity of a substance. As shown in Fig. 5B, we found that ANT-NPs displayed an obviously higher DPPH scavenging activity (60.12%) than free ANT (47.94%) and non-loaded NPs (7.15%) at the end of the entire digestion process. Herein, non-loaded NPs showed limited DPPH radical scavenging activity, whereas free ANT showed potent activity, which is ascribable to the presence of numerous H-donating phenolic hydroxyl groups in the ANT. Moreover, the antioxidant capacity of the ANT-NPs, free ANT, and non-loaded NPs were further evaluated and compared using the FRAP assay. Initially, the FRAP reduction capacity of free ANT (0.48%) was similar with that of ANT-NPs (0.50%), while the FRAP reduction capacity of ANT-NPs (0.35%) was higher than that of free ANT (0.17%) at the end of the entire digestion process.

The above retention rates and antioxidant assay results reveal that the ANT-NPs exhibit excellent physical and oxidative stability during simulated gastrointestinal digestion.

3.3.2 Storage studies. The application of ANT is limited due to their sensitivity to environmental temperature during storage.[34,35] This study measured the retention rates and antioxidant activities of ANT-NPs at −20, 4, 25, and 40 °C and compared the results with those of free ANTs and the non-loaded NPs. As shown in Fig. 6A, it could be found there was no significant difference in the retention rate of the ANT-NPs and free ANT at −20 and 4 °C. However, at 25 °C, the retention rate was significantly different, with values of 35.72 and 67.89% for the free ANT and ANT-NPs, respectively. Notably, at a stress temperature of 40 °C, the ANT-NPs presented 80.73% of the retention rate, while free ANT only have 22.54% at the end of the storage studies. These values indicated that the ANT-NPs displayed superior storage stability. Similar results were reported that the alginate capsules significantly improved the

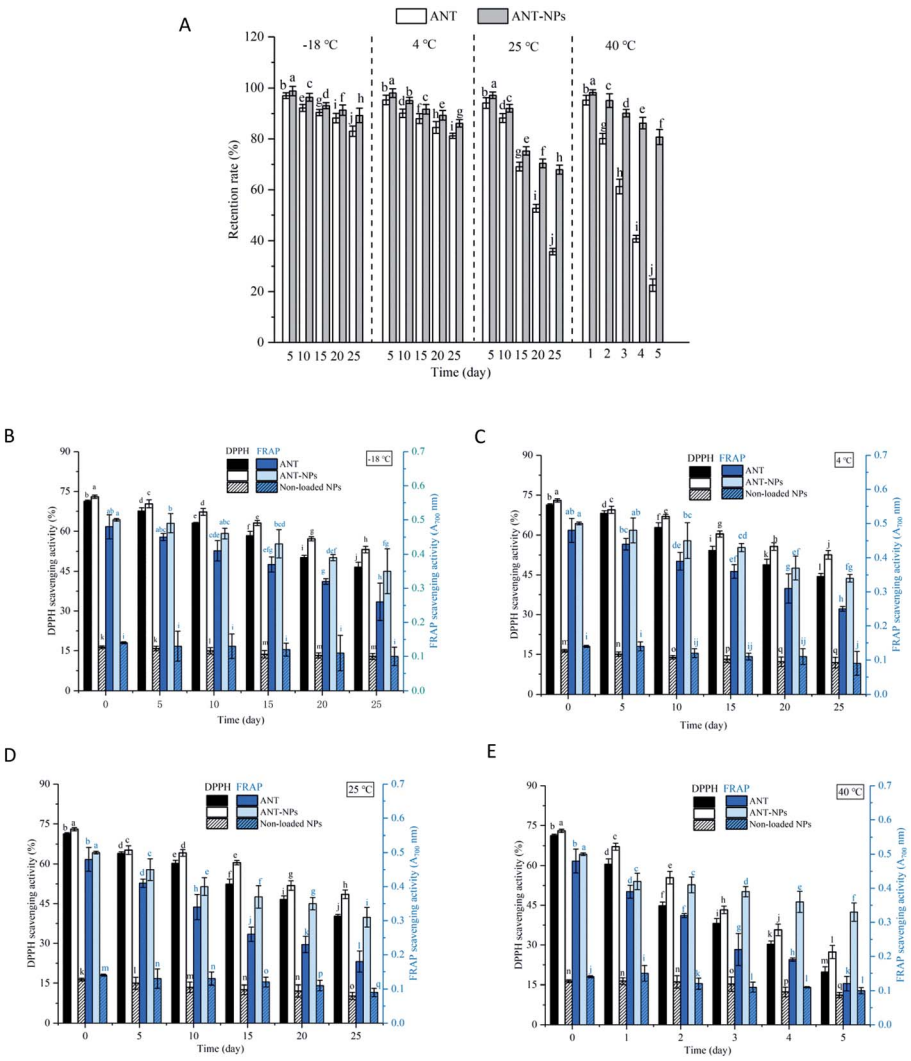

Fig. 6 (A) Retention rates and (B–E) antioxidant activities of various formulations during storage process. (B–D) Storage at temperatures of −18, 4, and 25 °C for 25 d; (E) storage at a temperature of 40 °C for 5 d. Data are expressed as means ± standard deviations ($n = 3$). Samples designated with different letters are significantly different (Duncan, $p < 0.05$).

stability of mulberry-extracted anthocyanins after freeze–thaw cycling and incubation at 45 °C for 60 days.[36]

The oxidative stabilities of free ANT, ANT-NPs, and the non-loaded NPs were subsequently assessed using the DPPH and FRAP assays. As shown in Fig. 6, the oxidative stabilities determined using these two assays exhibited the same trends. Our results revealed that the antioxidant activities of free ANT and ANT-NPs decreased with increasing storage temperature and time. Additionally, the decrease was observed to be more pronounced for free ANT, followed by ANT-NPs. The antioxidant activity of free ANT also decreased more rapidly at 40 °C (Fig. 6E). For example, the DPPH scavenging activity of ANT-NPs was 53.18, 52.56, 48.52 and 27.34% in the −20, 4, 25, and 40 °C treatment, respectively. In contrast, these figures were higher than those of equivalent free ANT, which were 46.5, 44.32, 40.27 and 19.77%, respectively. Interestingly, we found that the FRAP scavenging activities of ANT-NPs were also higher than those of free ANT at various storage temperatures. Notably, both the DPPH and FRAP scavenging activities of non-loaded NPs showed limited but not obvious reductions. We conclude that chitosan does not contribute to antioxidant activity, and that the significant enhancement in antioxidant activity is due to the inclusion of the ANT in the nanocapsules. These findings provide further evidence that nanoencapsulated ANT are more suited to storage than free ANT under various environmental conditions.

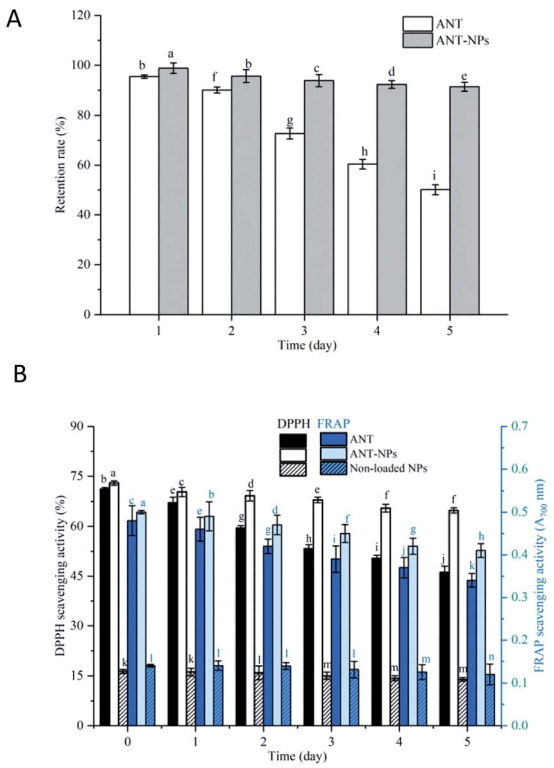

Fig. 7 (A) Retention rates and (B) antioxidant activities of various formulations after exposure to light. Data are expressed as means ± standard deviations (n = 3). Different letters over columns indicate significant differences between preparations (Duncan, $p < 0.05$).

3.3.3 Photo studies. Due to the photosensitivity of anthocyanins, white fluorescent light is an important factor to consider, especially when it comes to long-term storage and shelf-life. In this study, the retention rate and antioxidant activity of ANT and ANT-NPs under the photo condition were tracked for 5 days. As shown in Fig. 7A, under the photo condition, the protection effect of ANT-NPs on the stability of ANT began to express from the third day, and the retention rate of ANT (50.11%) was much lower than ANT-NPs (91.35%) on the last day, which demonstrated that the process of nanoencapsulation effectively reduce photo degradation of ANT. These results were in accordance with the report of Ge *et al.*,[37] who found that the chitosan hydrochloride and carboxymethyl chitosan nanocomplexes significantly improved the stability of anthocyanins against white fluorescent light. Lang *et al.*[38] also reported that better photo protective effect exhibited by α-casein and β-casein on blueberry anthocyanins. What's more, as we could see from Fig. 7B, in the presence of white fluorescent light, the DPPH scavenging activity of both free ANT and ANT-NPs decreased. However, the ANT-NPs had higher DPPH scavenging activity (64.81%) than the free ANT (46.15%) did at the end of photo treatment. In addition, the FRAP scavenging activity of ANT-NPs (0.41) was significantly higher than that of free ANT (0.34) and non-loaded NPs (0.12), which clearly indicates that the ANT-NPs are more oxidatively stable. Obviously, white fluorescent light had the great influence on the stability and antioxidant activity of the free ANT, but had no obvious effect on the ANT-NPs, indicating that the ANT-NPs have a protective effect on ANT against light-induced degradation.

4 Conclusions

In our study, response surface methodology (RSM) was used to optimise the preparation conditions of ANT-NPs with the chitosan (CS), tripolyphosphate (TPP) and anthocyanins (ANT). The achieved ANT-NPs with the best response exhibited maximum encapsulation efficiency (EE, 65.7%), minimum particle size (197 nm) and stable zeta potential (+42.7 mV). The successful load of ANT in ANT-NPs was clearly depicted through TEM and FT-IR spectroscopy. Compared with the free ANT, the ANT-NPs exhibited gradual release of ANT but sustained antioxidant activity during *in vitro* digestion. Additionally, it was also demonstrated that during storage and photo treatment, the ANT-NPs were able to preserve the retention rate and antioxidant activity of ANT against harsh environment. We therefore suggested the application of nanoencapsulation could be as a good alternative to enhance the physical and oxidant stability of ANT.

Conflicts of interest

The authors declare that there are no conflicts of interest.

Acknowledgements

Support for this study provided by the National Key Research and Development Program of China (Grant No. 2017YFD0400704-4) is gratefully acknowledged.

References

1 J. Zhang, J. Wu, F. Liu, L. Tong, Z. Chen, J. Chen, H. He, R. Xu, Y. Ma and C. Huang, *Eur. J. Pharmacol.*, 2019, **858**, 172500.
2 S. Hamedi and M. Koosha, *Appl. Clay Sci.*, 2020, **197**, 105770.
3 J. Y. Lee, Y.-u. Jo, H. Shin, J. Lee, S. U. Chae, S. K. Bae and K. Na, *Int. J. Pharm.*, 2020, **586**, 119597.
4 L. Xie, H. Su, C. Sun, X. Zheng and W. Chen, *Trends Food Sci. Technol.*, 2018, **72**, 13–24.
5 J. Koh, Z. Xu and L. Wicker, *Food Chem.*, 2020, **302**, 125343.
6 X. Sun, Z. Yan, T. zhu, J. Zhu, Y. Wang, B. Li and X. Meng, *Food Chem.*, 2019, **279**, 63–69.
7 S. Akhavan and S. M. Jafari, *Nanoencapsulation of Food Bioactive Ingredients*, 2017, pp. 223–260.
8 L. Chen, C. Gnanaraj, P. Arulselvan, H. El-Seedi and H. Teng, *Trends Food Sci. Technol.*, 2019, **85**, 149–162.
9 Y. Yang, J. Cheng, V. M. Garamus, N. Li and A. Zou, *J. Agric. Food Chem.*, 2018, **66**, 1067–1074.
10 Y. Li, H. Song, S. Xiong, T. Tian, T. Liu and Y. Sun, *Int. J. Biol. Macromol.*, 2018, **109**, 672–680.
11 M. Hamdi, R. Nasri, S. Li and M. Nasri, *Int. J. Biol. Macromol.*, 2020, **145**, 1140–1154.
12 J. Chi, J. Ge, X. Yue, J. Liang, Y. Sun, X. Gao and P. Yue, *LWT–Food Sci. Technol.*, 2019, **109**, 101–107.
13 L. Meng, J. Zhu, Y. Ma, X. Sun, D. Li, L. Li, H. Bai, G. Xin and X. Meng, *Food Biosci.*, 2019, **30**, 100413.
14 K. Prasad, D. Mondal, M. Sharma, M. G. Freire, C. Mukesh and J. Bhatt, *Carbohydr. Polym.*, 2018, **180**, 328–336.
15 T. Mohd, T. Belwal, I. D. Bhatt, V. Pande and S. K. Nandi, *Ind. Crops Prod.*, 2018, **117**, 66–74.
16 J. Wang, H. Li, Z. Chen, W. Liu and H. Chen, *Ind. Crops Prod.*, 2016, **89**, 152–156.
17 T. Wu, C. Grootaert, S. Voorspoels, G. Jacobs, J. Pitart, S. Kamiloglu, S. Possemiers, M. Heinonen, N. Kardum, M. Glibetic, G. Smagghe, K. Raes and J. Van Camp, *J. Funct. Foods*, 2017, **38**, 128–139.
18 D. Fasolo, B. Pippi, G. Meirelles, G. Zorzi, A. M. Fuentefria, G. von Poser and H. F. Teixeira, *J. Drug Delivery Sci. Technol.*, 2020, 101573.
19 I. Jazuli, Annu, B. Nabi, T. moolakkadath, T. Alam, S. Baboota and J. Ali, *J. Pharm. Sci.*, 2019, **108**, 3082–3090.
20 T. Moolakkadath, M. Aqil, A. Ahad, S. Sarim Imam, A. Praveen, Y. Sultana and M. Mujeeb, *Int. J. Pharm.*, 2020, 119125.
21 A. Grenha, B. Seijo and C. Remuñán-López, *Eur. J. Pharm. Sci.*, 2005, **25**, 427–437.
22 B. Hu, C. Pan, Y. Sun, Z. Hou, H. Ye, B. Hu and X. Zeng, *J. Agric. Food Chem.*, 2008, **56**, 7451–7458.
23 J. Liang, F. Li, Y. Fang, W. Yang, X. An, L. Zhao, Z. Xin, L. Cao and Q. Hu, *Colloids Surf., B*, 2011, **82**, 297–301.
24 A. Shetta, J. Kegere and W. Mamdouh, *Int. J. Biol. Macromol.*, 2019, **126**, 731–742.
25 J. Liang, H. Yan, X. Wang, Y. Zhou, X. Gao, P. Puligundla and X. Wan, *Food Chem.*, 2017, **231**, 19–24.
26 J. Feng, Y. Wu, L. Zhang, Y. Li, S. Liu, H. Wang and C. Li, *J. Agric. Food Chem.*, 2019, **67**, 10432–10447.
27 M. Luo, R. Zhang, L. Liu, J. Chi, F. Huang, L. Dong, Q. Ma, X. Jia and M. Zhang, *J. Food Eng.*, 2020, **284**, 110065.
28 M. Sharma, R. Sharma, D. K. Jain and A. Saraf, *Int. J. Biol. Macromol.*, 2019, **135**, 246–260.
29 S. N. Mazloomi, A. S. Mahoonak, M. Ghorbani and G. Houshmand, *J. Food Eng.*, 2020, **280**, 109976.
30 C. Tan, M. J. Selig and A. Abbaspourrad, *Carbohydr. Polym.*, 2018, **181**, 124–131.
31 J. Wu, Y. Wang, H. Yang, X. Liu and Z. Lu, *Carbohydr. Polym.*, 2017, **175**, 170–177.
32 I. Gheonea, I. Aprodu, A. Cîrciumaru, G. Râpeanu, G. E. Bahrim and N. Stănciuc, *J. Food Eng.*, 2021, **288**, 110166.
33 K. Tai, M. Rappolt, L. Mao, Y. Gao, X. Li and F. Yuan, *Food Hydrocolloids*, 2020, **99**, 105355.
34 K. Sarabandi and S. M. Jafari, *J. Food Eng.*, 2020, **286**, 110131.
35 M. Zembyla, A. Lazidis, B. S. Murray and A. Sarkar, *J. Food Eng.*, 2020, **281**, 109991.
36 S. Kanokpanont, R. Yamdech and P. Aramwit, *Artif. Cells, Nanomed., Biotechnol.*, 2018, **46**, 773–782.
37 J. Ge, P. Yue, J. Chi, J. Liang and X. Gao, *Food Hydrocolloids*, 2018, **74**, 23–31.
38 Y. Lang, H. Gao, J. Tian, C. Shu, R. Sun, B. Li and X. Meng, *LWT–Food Sci. Technol.*, 2019, **115**, 108434.